2017 21st International Conference on Process Control (PC)
June 6–9, 2017, Štrbské Pleso, Slovakia

Combined flow and pressure control for industrial pumps with adaptive MPC

Sebastian Leonow
Ruhr-University Bochum,
Automatic Control and Systems Theory,
Email: sebastian.leonow@rub.de

Fabian Wollenhaupt
Ruhr-University Bochum,
Automatic Control and Systems Theory,
Email: fabian.wollenhaupt@rub.de

Martin Mönnigmann*
Ruhr-University Bochum,
Automatic Control and Systems Theory,
Email: martin.moennigmann@rub.de

***Abstract*—We show a simple adaptive linear MPC is suitable to simultaneously control flow rates and pressures in hydraulic processes over wide operating ranges. The predictive controller is adaptive in that the nonlinear process model is re-linearized whenever setpoint changes occur. While its implementation is hardly more complicated than for linear MPC and no additional signals or observers are required, the adaptive controller improves the performance considerably. We apply the proposed approach to the simultaneous flow rate and pressure control for a side-channel pump, and compare it to standard linear MPC and multivariate PID control by applying all three methods to a laboratory setup. As a side-effect, the paper contains a nonlinear model of a side-channel pump and process that is suitable as a benchmark for other control concepts. In contrast to centrifugal pumps, models of this type are not available in the literature for side-channel pumps to the knowledge of the authors.**

I. Introduction

The problem of simultaneous control of pressure and flow in a hydraulic process arises in a variety of applications. An example is found in reverse osmosis (RO) units for seawater desalination or raw water purification. These processes pose a challenging control problem due to the strong coupling between the controlled variables and the inherent nonlinearities. Two control loops with independently tuned controllers are likely to show poor performance, or even fail, as both controllers strongly disturb each other. Model predictive control is an obvious alternative, since it can be applied to multi-input-multi-output (MIMO) processes by design, and since it naturally can cope with constraints. Linear MPC, however, is not an obvious choice, as hydraulic processes are nonlinear systems that typically have to be run at varying operating points. However, since hydraulic systems are often run at varying steady states, but after all at steady state most of the time, a nonlinear MPC setup appears to be unreasonably complex. Similar arguments apply to linear MPC with time-variant models (see, e.g., Falcone (2008), Drews (2009) and Henriksen (2010) for successful applications).

We therefore propose to use a nonlinear process model and adaptive linear MPC, where 'adaptive' here refers to the simple idea of re-computing the linearized process model whenever a setpoint change occurs. We will apply this idea to a laboratory setup with a side-channel pump, which incidentally may serve as a model system for a typical RO unit process (see Fig. 1 and e.g. Gambier (2006)).

The proposed adaptive controller, a linear MPC, and two PI/PID controllers are applied to a laboratory setup, which is described in Sec. II. Section III describes the nonlinear plant model, which is parametrized for the specific laboratory setup in Sec. III-D. We outline our MPC approach and tune PI/PID controllers for comparison in Sec. IV. Results and a comparison of the controllers are given in Sec. V.

II. Process description

The considered class of hydraulic processes consists of a feedwater pump with variable speed drive, a pressure control valve and sensors for pressure and flow rate. The objective

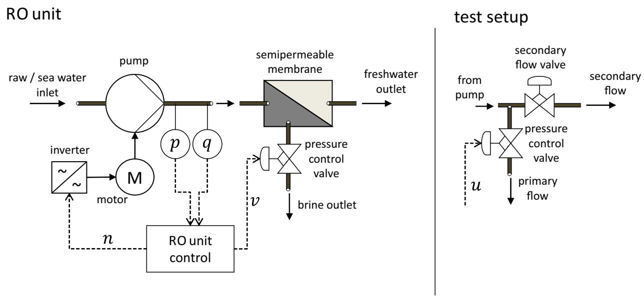

Fig. 1. Typical RO unit setup (left) and test setup (right)

is to simultaneously control pressure and flow rate with a controller that is suitable for a wide range of setpoints. Figure 1 depicts a sample RO unit setup in the left diagram (cf. e.g. Gambier (2006)). The right diagram depicts the subsitute test setup that we used for evaluation. The two controlled variables are the pressure p and the flow rate q, both on the feedwater side, immediately downstream of the feedwater pump. Process inputs are the feedwater pump speed n and the control valve setting v. The secondary flow in the test setup (Fig. 1 right) is used to simulate the semipermeable membrane, i.e. the freshwater output, and acts as disturbance to the control. Because the considered process requires high pressures at relatively low flow rates, centrifugal pumps are not well suited. We use a side-channel pump instead, as it features high pressure outputs and a steep pressure to flow characteristic (cf. Fig. 4(a) in Sec. III-D). Details on the control hardware in the laboratory setup are given in Sec. III-D.

III. Nonlinear modelling

The process model includes nonlinear dynamic pump and process characteristics as well as models of the sensing equipment, combined to a model in a Hammerstein-like structure. The model consists of four parts: a feedwater pump, an actuated control valve, a pressure sensor and a flow rate sensor. The individual model parts are combined to the process model as shown in Fig. 2. We will outline the mathematical modelling

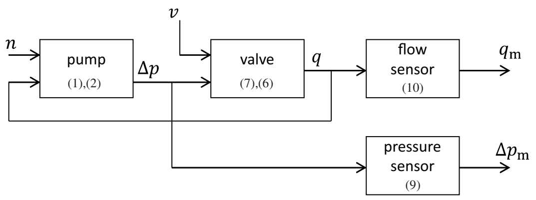

Fig. 2. Combined nonlinear dynamic plant model. Numbers refer to equations stated in the text.

of each part separately in the remainder of Sec. III. The parametrization of the models is discussed in Sec. III-D.

A. Model of the side-channel pump

Due to the complex geometry of the side-channel pump, modelling requires more parameters than typically needed for centrifugal pumps. Literature on side-channel pumps is not as comprehensive as for centrifugal pumps. However, some publications can be found in the German literature (e.g. Grabow (1996), Surek (1997)). We follow Surek (1997) in modelling the pressure-to-flow relation by

$$p(n,q,p_{\mathrm{in}}) = \frac{k_{\mathrm{p},1}\cdot n\cdot\left(1-\frac{q}{q_{\max}(n)}\right)^{m}}{k_{\mathrm{p},2}} - k_{\mathrm{p},3}\cdot q + p_{\mathrm{in}}\ , \quad (1)$$

where

$$\begin{aligned} k_{\mathrm{p},1} &= \rho\cdot\pi\cdot 30^{-1}\cdot\gamma_0\cdot r_o\cdot A_{\mathrm{sc}}\cdot\left(r_o^4-r_i^4\right)\\ k_{\mathrm{p},2} &= r_m\cdot r_{\mathrm{sc}}^2\cdot\left(\pi\cdot\left(r_o^2-r_m^2\right)-\frac{s_{\mathrm{b}}\cdot z_{\mathrm{b}}}{\sin\beta_{\mathrm{b}}}\cdot(r_o-r_m)\right)\\ k_{\mathrm{p},3} &= \zeta\cdot\frac{\rho}{2}\cdot\alpha_{\mathrm{sc}}\cdot\left(2\cdot\pi\cdot r_{\mathrm{sc}}^2\right)^{-1} \end{aligned} \quad (2)$$

and $r_{\mathrm{m}} = 0.5\cdot(r_{\mathrm{o}}+r_{\mathrm{i}})$. In (1), $q_{\max}(n)$ is short for $q_{\max}(n) = q_{\mathrm{des}}\cdot n\cdot n_{\mathrm{des}}^{-1}$ with q_{des} being the maximal flow rate at design speed n_{des}. The parameters γ_0, m and ζ depend on the specific rotational speed n_{q}, a dimensionless number that characterizes the geometric pump and impeller design (see. e.g. Gulich (2007) p. 82). Surek (1997) published a diagram that shows the graphs of the functions $\gamma_0(n_{\mathrm{q}})$, $m(n_{\mathrm{q}})$ and $\zeta(n_{\mathrm{q}})$. We derived the following polynomials from this diagram:

$$\begin{aligned} m(n_{\mathrm{q}}) &= -4.6339\cdot 10^{-5}\cdot n_{\mathrm{q}}^6 + 0.00167\cdot n_{\mathrm{q}}^5 - 0.02364\cdot n_{\mathrm{q}}^4\\ &\quad +0.16126\cdot n_{\mathrm{q}}^3 - 0.511\cdot n_{\mathrm{q}}^2 + 0.7553\cdot n_{\mathrm{q}} - 0.3485\\ \gamma_0(n_{\mathrm{q}}) &= \frac{1}{5}\left(795.4\cdot e^{-2.415\cdot n_{\mathrm{q}}} + 2.049\cdot e^{-0.221\cdot n_{\mathrm{q}}}\right)\\ \zeta(n_{\mathrm{q}}) &= \frac{1}{5}\left(-4\cdot 10^{-5}\cdot n_{\mathrm{q}}^6 + 0.00158\cdot n_{\mathrm{q}}^5 - 0.0246\cdot n_{\mathrm{q}}^4\right.\\ &\quad \left. +0.1886\cdot n_{\mathrm{q}}^3 - 0.6907\cdot n_{\mathrm{q}}^2 + 0.751\cdot n_{\mathrm{q}} + 1.425\right) \end{aligned} \quad (3)$$

The remaining parameters from (1) and (2) are given in Sec. III-D.

B. Valve and pipe models

We use an actuated control valve to simulate the freshwater outflow. The valve is modelled in a first order Hammerstein-like structure to account for the effects of fluid inertia. The nonlinear static part is described by the pressure loss equation (e.g. Gulich (2007), p. 5)

$$p_{\Delta}(\zeta_{\mathrm{v}},q) = \zeta_{\mathrm{v}}\cdot\frac{\rho}{2}\cdot\left(\frac{q}{A_{\mathrm{v}}}\right)^2 , \quad (4)$$

where the valve coefficient ζ_{v} and the valve cross section A_{v} depend on the valve opening. We substitute (4) by

$$p_{\Delta}(q,v) = k_{\mathrm{v}}(v)\cdot q^2 \quad (5)$$

and measure $k_{\mathrm{v}}(v)$ for the real valve (see Sec. III-D). We anticipate $k_{\mathrm{v}}(v)$ can be approximated by a piecewise affine function

$$k_{\mathrm{v}}(v) = \frac{v - v_{\mathrm{f}}(i-1)\cdot(k_{\mathrm{v,f}}(i)-k_{\mathrm{v,f}}(i-1))}{v_{\mathrm{f}}(i)-v_{\mathrm{f}}(i-1)} + k_{\mathrm{v,f}}(i-1)\ , \quad (6)$$

where $v_{\mathrm{f}}(i)$ and $k_{\mathrm{v,f}}(i)$ hold the i-th measured data point (see Fig. 4(b) for the data points and the resulting function). The fluid inertia is accounted for with a first order lag $T_{\mathrm{i}}\dot{q}(t) = -q(t)+u(t)$ (see. e.g. Gulich (2007), p. 4), where the input $u(t)$ is given by (5) solved for q:

$$\dot{q}(t) = \frac{1}{T_{\mathrm{i}}}\left(-q(t)+\sqrt{\Delta p(t)\cdot k_{\mathrm{v}}(v(t))^{-1}}\right) \quad (7)$$

C. Sensor models

Sensing equipment may introduce dominant time constants, in particular in fast pressure control loops, which can significantly reduce control quality when ignored in the controller design. Moreover, pressure and flow rate sensors are typically connected to a process control system (PCS), which may introduce deadtimes due to computation and communication. However, the time constants of the sensing equipment and the PCS cycle times are independent of the operating point. Since the nonlinearities of the process have been covered by the previously described pump and valve characteristics, it suffices to model the sensors with linear, time invariant models with constant deadtimes. Based on observations of the sensor dynamics we choose a second order plus deadtime system

$$\ddot{y}(t) + a_2\dot{y}(t) + a_1 y(t) = b_1\dot{u}(t-T_{\mathrm{D}}) + a_1 u(t-T_{\mathrm{D}}) \quad (8)$$

and apply an identification method proposed by Wang (2001), which is based on step responses. Details on the parametrization are given in the following Sec. III-D.

D. Application to the test bench

We will focus on the application of the models to the specific process already sketched in Sec. II from here on. The test setup consists of a Flowserve/SIHI AKH 1201 side-channel pump, attached to a variable speed controlled induction motor with inverter. The discharge port is fitted with

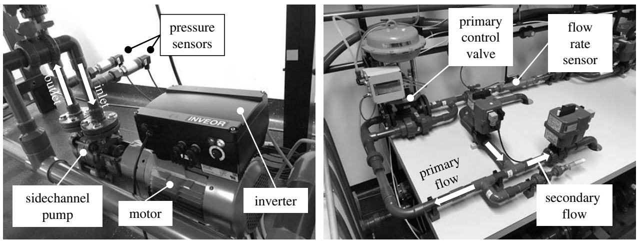

Fig. 3. Hardware layout of the plant simulator and FLOWSERVE/SIHI AKH 1201 side-channel pump

a pressure sensor; a flow rate sensor is fitted downstream. A standard industrial PCS is used to handle sensor and actuator signals. The control algorithms are executed on a PC running MATLAB / SIMULINK that is connected to the PCS via OPC[1] using the Simulink OPC toolbox. Figure 3 shows the side-channel pump and the laboratory process layout.

1) Identification of pump and valve models: .The parameters of the pump model (1), in particular the radii r_o, r_i and r_{sc}, depend on the actual pump design and are typically not published. This also holds for the blade thickness s_{b}, the blade angle β_{b}, the blade count z_{b}, the circumferential angle of the side-channel α_{sc} and the side-channel surface area A_{sc}. In order to determine these parameters without disassembling the pump, we measured the head to flow relation (with the head defined by $h = (p - p_{\mathrm{in}}) \cdot (\rho \cdot g)^{-1}$) for four different speeds n, and fitted the unknown parameters using a brute-force optimization. We included the constraints $r_{\mathrm{i}} \cdot r_{\mathrm{o}}^{-1} \in [0.35, 0.45]$

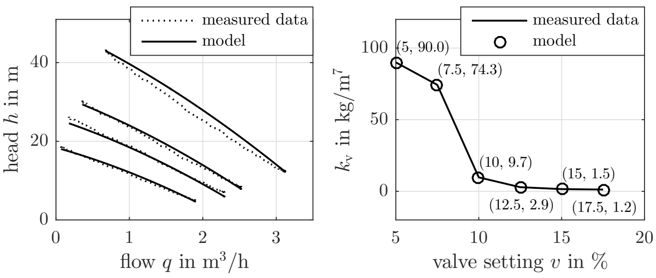

(a) (b)

Fig. 4. (a)Verification of the pump model (1) at speeds (from bottom to top) $n = 1100\ \mathrm{min}^{-1}$, $n = 1300\ \mathrm{min}^{-1}$, $n = 1450\ \mathrm{min}^{-1}$, $n = 1800\ \mathrm{min}^{-1}$; (b) Valve characteristics (6) with value pairs $(v_{\mathrm{f}}, k_{\mathrm{v,f}})$.

and $r_{\mathrm{sc}} \cdot r_{\mathrm{o}}^{-1} \in [0.15, 0.35]$ to ensure compliance with the geometry of the actual pump. The parametrized pump model is compared to the measured data in Fig. 4(a), which confirms a sufficient model quality. The resulting parameters are given in Table I. The piecewise affine valve characteristic (6) was parametrized with the data points shown in Fig. 4(b). The fluid inertia is very low due to the short pipings. We estimated the corresponding time constant in (7) to $T_{\mathrm{i}} = 0.1$ s.

2) Identification of the sensor models: .The identification of the sensor models (8) was performed on the basis of a

[1]OPC: OLE (Object Linking and Embedding) for Process Control.

TABLE I
PUMP MODEL PARAMETERS

param.	value	unit	param.	value	unit
ρ	1000	kg/m^3	s_{b}	0.005	m
r_{o}	0.07	m	z_{b}	18	
r_{i}	0.0245	m	β_{b}	90	°
r_{sc}	0.0227	m	α_{sc}	200	°
A_{sc}	8.0942e-4	m^2	q_{des}	0.0018	m^3/s
n_{q}	8.5		n_{des}	1450	min^{-1}

step response measurement. Applying the method proposed by Wang (2001) yields the pressure sensor transfer function

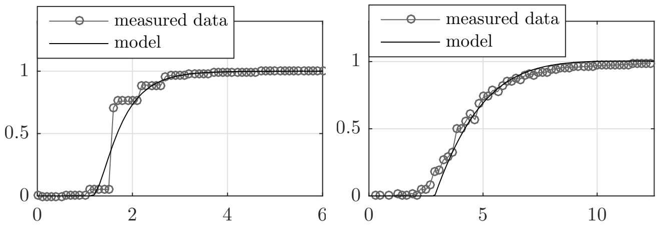

(a) (b)

Fig. 5. Pressure (a) and flow rate sensor (b) step responses

$$G_{\mathrm{s},p}(s) = \frac{12.09 \cdot e^{-1.5 \cdot s}}{s^2 + 7.928 \cdot s + 12.09} \tag{9}$$

and the flow rate sensor transfer function

$$G_{\mathrm{s},q}(s) = \frac{(0.4776 \cdot s + 0.3723) \cdot e^{-3 \cdot s}}{s^2 + 1.096 \cdot s + 0.3723} \ , \tag{10}$$

that represent the measured responses sufficiently precise for our purposes (cf. Fig. 5).

3) Linearized process model: .While the proposed adaptive MPC and the state observer depend on the nonlinear model, a linear model is required for the linear MPC and the PID controller tuning. We choose the steady state operating point

$$\begin{aligned} v_0 &= 8.5\ \% \ , \ n_0 = 1450\ \mathrm{min}^{-1} \ , \\ q_0 &= 2.05 \cdot 10^{-4}\ \mathrm{m}^3/\mathrm{s} \ , \ p_0 = 2.58 \cdot 10^5\ \mathrm{Pa} \end{aligned} \tag{11}$$

for the linearization.

The pump model (1) yields two constants when linearized, describing the reaction of p to a change in q and n:

$$k_{\mathrm{p},q} = \frac{k_{\mathrm{p},1} \cdot m \cdot n_{\mathrm{des}} \cdot n_0 \cdot \left(1 - \frac{n_{\mathrm{des}} \cdot q_0}{n_0 \cdot q_{\mathrm{des}}}\right)^{m-1}}{-k_{\mathrm{p},2} \cdot q_{\mathrm{des}}} - 2 \cdot k_{\mathrm{p},3} \cdot q_0 \tag{12}$$

$$\begin{aligned} k_{\mathrm{p},n} =& \frac{k_{\mathrm{p},1} \cdot n_0 \cdot \left(\frac{q_{\mathrm{des}} \cdot n_0 - q_0 \cdot n_{\mathrm{des}}}{q_{\mathrm{des}} \cdot n_0}\right)^m}{k_{\mathrm{p},2} \cdot (q_{\mathrm{des}} \cdot n_0 - q_0 \cdot n_{\mathrm{des}})} \\ & \cdot (2 \cdot q_{\mathrm{des}} \cdot n_0 + (m+2) \cdot q_0 \cdot n_{\mathrm{des}}) \end{aligned} \tag{13}$$

Linearizing the valve equations (6) and (7) yields two linear first order differential equations, describing the flow reaction to a change in v and p. It is convenient to state these equations as their equivalent transfer funtions for our purposes. The transfer functions read

$$G_{\mathrm{v},v}(s)=\frac{\Delta q(s)}{\Delta v(s)}=G_{\mathrm{i}}(s)\cdot\underbrace{\frac{-p_0\cdot k_{\mathrm{v}}(v_0)^{-2}}{2\cdot\sqrt{p_0\cdot k_{\mathrm{v}}(v_0)^{-1}}}\cdot\left.\frac{\mathrm{d}k_{\mathrm{v}}(v)}{\mathrm{d}v}\right|_{\mathrm{OP}}}_{k_{\mathrm{v},v}} \tag{14}$$

and

$$G_{\mathrm{v},p}(s)=\frac{\Delta q(s)}{\Delta p(s)}=G_{\mathrm{i}}(s)\cdot\underbrace{\left(2\cdot k_{\mathrm{v},0}\cdot\sqrt{p_0\cdot k_{\mathrm{v}}(v_0)^{-1}}\right)^{-1}}_{k_{\mathrm{v},p}}, \tag{15}$$

where $G_{\mathrm{i}}(s)=(T_{\mathrm{i}}s+1)^{-1}$. Note that the expression $\frac{\mathrm{d}k_{\mathrm{v}}(v)}{\mathrm{d}v}$ is negative over the valve operating range (see Fig. 4(b)), so that (14) shows correct physical behaviour (i.e. opening the valve leads to higher flow rate). Figure 6 outlines the linear model scheme. The linearized model is transformed into a discrete-time state-space representation

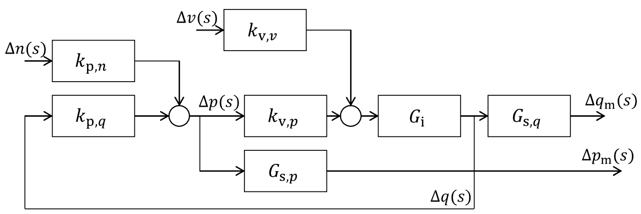

Fig. 6. Linearized model scheme

$$\begin{aligned} x(k+1) &= \boldsymbol{A}(\mathrm{OP})\cdot x(k)+\boldsymbol{B}(\mathrm{OP})\cdot u(k)\\ y(k) &= \boldsymbol{C}\cdot x(k)\ , \end{aligned} \tag{16}$$

with the state vector

$$\boldsymbol{x}=(x_{q,1},\dots,x_{q,8},x_{p,1},\dots,x_{p,5},x_{\mathrm{i}})^T$$

that contains the states of the flow rate ($x_{q,i}$ with $i=1,\dots,8$), of the pressure sensor models ($x_{p,i}$ with $i=1,\dots,5$), and of the flow inertia model (state x_{i}). Eight states $x_{q,i}$ and five states $x_{p,i}$ result because of the dead times, which are integer multiples of the discretization time $T_{\mathrm{d}}=0.5$ s in both cases. The input vector $u=(v,n)^T$ holds valve position and pump speed, the output vector $y=(q,p)^T$ holds the feedwater flow rate and the feedwater (pump discharge) pressure. The abbreviation OP in (16) is meant to indicate that the matrices are evaluated at the steady state that corresponds to (11) for linear MPC and PI/PID control, and at various steady states for the adaptive MPC approach detailed in Sec. IV. Note that (16) could be transformed to a time-variant model by substituting OP $=$ OP$(k)=v(k),n(k),q(k),p(k)=\begin{pmatrix}u(k) & x_8(k) & x_{13}(k)\end{pmatrix}$ into $\boldsymbol{A}(\mathrm{OP})$, $\boldsymbol{B}(\mathrm{OP})$, $\boldsymbol{C}(\mathrm{OP})$ and denoting the resulting matrices $\boldsymbol{A}(k)$, $\boldsymbol{B}(k)$, $\boldsymbol{C}(k)$, respectively[2].

[2] We avoid this notation, because we are not using the time-variant model. In contrast, (16) is used with time-invariant matrices that correspond to the steady state operating point (11) in the reference linear MPC implementation, the observer, and PID tuning, and the matrices in (16) are adjusted whenever the setpoint changes in the adaptive MPC proposed here.

To compose the matrices in (16), the sensor models (10) and (9) are transformed into discrete-time state-space models with matrices $(\boldsymbol{A}_{\mathrm{s},q},\boldsymbol{b}_{\mathrm{s},q},\boldsymbol{c}_{\mathrm{s},q})$ and $(\boldsymbol{A}_{\mathrm{s},p},\boldsymbol{b}_{\mathrm{s},p},\boldsymbol{c}_{\mathrm{s},p})$, respectively, by using standard methods. The flow inertia model contains the Δq feedback loop as depicted in Fig. 6 and reads

$$\dot{x}(t)=\left(T_{\mathrm{i}}^{-1}\left(k_{\mathrm{p},q}\cdot k_{\mathrm{v},p}-1\right)\right)x(t)+T_{\mathrm{i}}^{-1}u(t) \tag{17}$$

The discretization of (17) yields the (scalar) state-space matrices a_{i}, b_{i} and c_{i}. The three linear models are combined to yield the matrices

$$\boldsymbol{A}(\mathrm{OP})=\left(\begin{array}{cc|cc|c} \boldsymbol{A}_{\mathrm{s},q} & \boldsymbol{0} & & & \begin{pmatrix}c_{\mathrm{i}}(\mathrm{OP})\\0\end{pmatrix}\\ \boldsymbol{c}_{\mathrm{s},q} & \boldsymbol{0} & \multicolumn{2}{c|}{\boldsymbol{0}^{8\times5}} & 0\\ \boldsymbol{0} & \boldsymbol{I}^{5\times6} & & & \boldsymbol{0}\\ \hline & & \boldsymbol{A}_{\mathrm{s},p} & \boldsymbol{0} & \begin{pmatrix}k_{\mathrm{p},q}(n_0,q_0)\cdot c_{\mathrm{i}}(\mathrm{OP})\\0\end{pmatrix}\\ \multicolumn{2}{c|}{\boldsymbol{0}^{5\times8}} & \boldsymbol{c}_{\mathrm{s},p} & \boldsymbol{0} & \boldsymbol{0}\\ & & \boldsymbol{0} & \boldsymbol{I}^{2\times3} & \boldsymbol{0}\\ \hline \multicolumn{2}{c|}{\boldsymbol{0}^{1\times8}} & \multicolumn{2}{c|}{\boldsymbol{0}^{1\times5}} & a_{\mathrm{i}}(\mathrm{OP}) \end{array}\right),$$

$$\boldsymbol{B}(\mathrm{OP})=\left(\begin{array}{c|c} \boldsymbol{0}^{8\times1} & \boldsymbol{0}^{8\times1}\\ \hline 0 & k_{\mathrm{p},n}(n_0,q_0)\cdot\boldsymbol{b}_{\mathrm{s},p}\\ \hline \boldsymbol{0}^{4\times1} & \boldsymbol{0}^{4\times1}\\ \hline k_{\mathrm{v},v}(v_0,p_0)\cdot b_{\mathrm{i}}(\mathrm{OP}) & k_{\mathrm{v},p}(v_0,p_0)\cdot k_{\mathrm{p},n}(n_0,q_0)\cdot b_{\mathrm{i}}(\mathrm{OP}) \end{array}\right),$$

$$\boldsymbol{C}=\begin{pmatrix}\boldsymbol{0}^{2\times7} & \begin{pmatrix}1\\0\end{pmatrix} & \boldsymbol{0}^{2\times4} & \begin{pmatrix}0\\1\end{pmatrix} & \boldsymbol{0}^{2\times1}\end{pmatrix}, \tag{18}$$

with $\boldsymbol{I}^{i\times j}=\begin{cases}0 \text{ if } i\neq j\\ 1 \text{ if } i=j\end{cases}$ and $\boldsymbol{0}$ being a zero matrix of appropriate dimension where not explicitly stated. The abbreviation OP is understood as in (16).

IV. Model predictive control with on-line linearization

We use a standard linear MPC approach as given e.g. in Maciejowski (2002). The cost function

$$J(k)=\sum_{j=H_w}^{H_p}||\tilde{e}(k+j|k)||^2_{\boldsymbol{Q}}+\sum_{j=0}^{H_u-1}||\delta\tilde{u}(k+j|k)||^2_{\boldsymbol{R}} \tag{19}$$

is to be minimized in every time step, while only the first element of the resulting optimal input trajectory is applied to the plant. In (19), $\tilde{e}(k)=w(k)-\tilde{y}(k)$ is the predicted control error, $\delta\tilde{u}$ is the predicted input variation per sample and $\boldsymbol{Q}$ and $\boldsymbol{R}$ are weighting matrices for control error and input variation, respectively. The minimization is subject to the process dynamics (16) and the constraints

$$\begin{aligned} \begin{pmatrix}5, & 600\end{pmatrix}^T \leq\ & u(k) && \leq \begin{pmatrix}17, & 1800\end{pmatrix}^T\\ T_{\mathrm{d}}\cdot\begin{pmatrix}-1, & -50\end{pmatrix}^T \leq\ & \delta u(k) && \leq T_{\mathrm{d}}\cdot\begin{pmatrix}1, & 50\end{pmatrix}^T\\ \begin{pmatrix}0, & 0\end{pmatrix}^T \leq\ & y(k) && \leq \begin{pmatrix}4\cdot10^{-4}, & 1\cdot10^{7}\end{pmatrix}^T \end{aligned} \tag{20}$$

The constraints (20) reflect the feasible process boundaries and ensure that pump and valve are operated in their defined operating ranges (cf. Fig. 4(a) and 4(b)). A dead-beat observer is used to estimate the full state vector from the measurements:

$$\begin{aligned}\hat{x}(k+1)=(\boldsymbol{A}(\mathrm{OP})-\boldsymbol{L}(\mathrm{OP})\cdot\boldsymbol{C})\cdot\hat{x}(k)+\boldsymbol{B}(\mathrm{OP})\cdot u(k)\\ +\boldsymbol{L}(\mathrm{OP})\cdot y(k)\ ,\end{aligned}$$

using the same state space model as the controller. The tuning of the MPC is performed manually. We choose the weigthing matrices as follows:

$$\boldsymbol{Q} = \begin{pmatrix} 1 \cdot 10^{10} & 0 \\ 0 & 0.01 \end{pmatrix} \quad \boldsymbol{R} = \begin{pmatrix} 0.01 & 0 \\ 0 & 0.01 \end{pmatrix} .$$

The entries in $\boldsymbol{Q}$ consider the physical units of q and p and therefore differ in several orders of magnitude. The flow rate is weighted approx. 1000 times more strongly than the pressure, as we received best results with this tuning. We choose the horizon lengths to $H_p = 50$, $H_w = 20$ and $H_u = 10$, again, as these settings showed best results during the tests.

A. Adaptive MPC

We briefly mentioned in Sec. III-D the matrices $\boldsymbol{A}(\mathrm{OP})$, $\boldsymbol{B}(\mathrm{OP})$ stated in (18) can be interpreted as time-variant matrices $\boldsymbol{A}(k)$, $\boldsymbol{B}(k)$ by substituting $\mathrm{OP} = \mathrm{OP}(k) = \big(u(k) \quad x_8(k) \quad x_{13}(k)\big)$. Using the resulting time-variant system $x(k+1) = \boldsymbol{A}(k)x(k) + \boldsymbol{B}(k)u(k)$ essentially results in an MPC with linearizations along trajectories (see e.g. Falcone (2008), Drews (2009) and Henriksen (2010)). In contrast, we here re-calculate the matrices (18) only if the setpoint $w = (q, p)$ changes, which results in a setpoint-adapted linear MPC. Note this is considerably simpler for two reasons. For one, a linear MPC implementation can obviously be used after minor extensions. Secondly, no measurements of y, x or u are required, but the adapted matrices only depend on the desired new setpoint w (see Fig. 7), which is known and does not need to be measured or estimated.

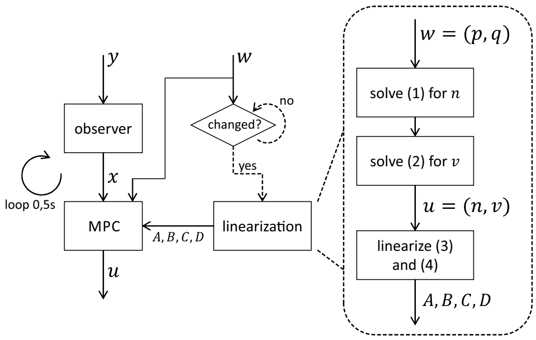

Fig. 7. MPC and linearization interaction

B. MIMO PID controller for comparison

An analysis of the relative gain array Λ (e.g. Skogestad (2007), p. 82) of the process at the nonimal OP (11) yields

$$\Lambda = K \cdot \mathrm{inv}(K)^T = \begin{pmatrix} 0.894 & 0.106 \\ 0.106 & 0.894 \end{pmatrix} , \tag{21}$$

with K being the steady state gain matrix of the process. Λ reveals that a diagonal pairing of the in- and outputs is optimal. We thus choose the first control circuit so that it controls the flow q by acting on the valve opening v. The second control circuit is chosen so that it controls the pressure p by acting on the pump speed n. We compensate the slow system dynamics in both systems with a controller zero of a realizable PID controller

$$C(z) = K_\mathrm{c} \cdot \frac{(z - p_{\mathrm{c},1}) \cdot (z - p_{\mathrm{c},2})}{(z-1) \cdot (z - p_{\mathrm{c,f}})} ,$$

with zeroes $p_{\mathrm{c},1}$ and $p_{\mathrm{c},2}$ and filter constant $p_{\mathrm{c,f}}$. In case of the flow rate control loop, there is only one real pole, and $p_{\mathrm{c},2}$ and $p_{\mathrm{c,f}}$ can be set to zero. In the pressure control loop, the two slowest poles are compensated by $p_{\mathrm{c},1} = 0.357$ and $p_{\mathrm{c},2} = 0.053$. We choose a filter time constant of $T_\mathrm{f} = 0.1$ s, which yields $p_{\mathrm{c,f}} = 0.0067$. The second tuning step involves choosing the controller gain K_c so that desired control properties are met. We tuned both control loops with a damping of the dominant pair of poles of approximately 0.5 for a reasonable compromise between speed and robustness. This yields $K_\mathrm{c} = 0.004$ for the pressure control loop and $K_\mathrm{c} = 1.62 \cdot 10^3$ for the flow rate control loop.

V. Results

We compare three control variants: (i) the adaptive MPC described in Sec. IV, (ii) a standard linear MPC based on the model (18), linearized at the nominal OP (11) and (iii) the PI / PID controller described in Sec. IV-B, which is also based on the model linearized at the nominal OP (11). We measure the controller performance with the integral abolute control error (IAE)

$$IAE = \sum_i |w(i) - y(i)| \tag{22}$$

for all time points i. We evaluated a "nominal" control scenario with average setpoint changes and a scenario where large setpoint steps occurs.

A. Nominal operation scenario

The IAE was measured in a long term test with several moderate setpoint changes to cover different coupling effects between the two controlled variables. Figure 8 shows the time series of the evaluation scenario. Stable control is achieved

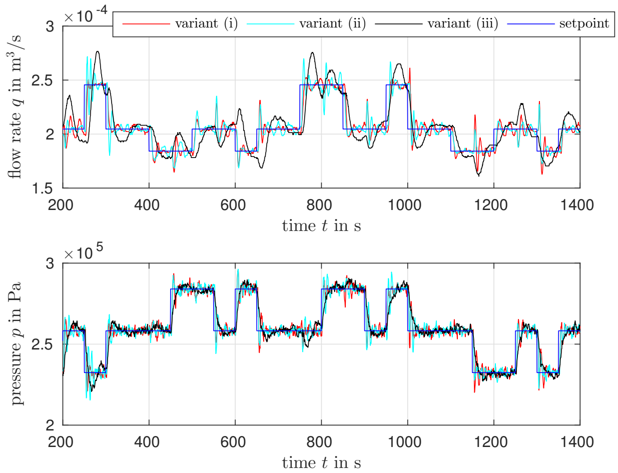

Fig. 8. Control quality during nominal operation

with all three control variants, as evident from Fig. 8. Table II summarizes the IAE and cost function values. The proposed adaptive MPC (variant (i)) controls the system slightly more efficiently than the standard MPC (variant (ii)) and makes better use of the coupled inputs. This observation is confirmed by the lower IAE values and a significantly lower cost $\sum_k J(k)$ for variant (i). Both MPC variants very clearly outperform the decentralized PID control (variant (iii)).

TABLE II
IAE FOR THE SCENARIO FROM FIG. 8

variant	IAE for p in %	IAE for q in %	$\sum_k J(k)$ in %
(i)	83	49.6	24.1
(ii)	87.4	50.1	100
(iii)	100	100	-

B. Large setpoint variation

The advantages of the online linearized MPC become more obvious when larger variations from the nominal operating point occur. Figure 9 depicts a time series around a large setpoint increase in both controlled variables. In this scenario,

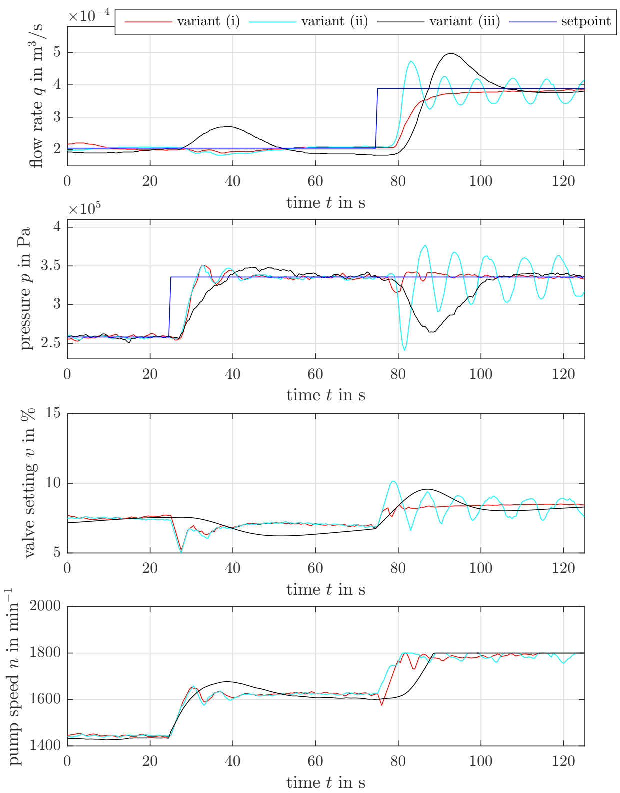

Fig. 9. Control quality with large setpoint step

the standard MPC (variant (ii)) fails as it runs into an undesired limit cycle when the large setpoint increase at $t = 75$ s occurs. The other two variants handle this situation well, while the online-linearized MPC again outperforms the PID control significantly. The IAE and cost function values summarized in Tab. III corroborate this result. The proposed adaptive

TABLE III
IAE FOR THE SCENARIO FROM FIG. 9

variant	IAE for p in %	IAE for q in %	$\sum_k J(k)$ in %
(i)	39.8	49.8	43.1
(ii)	93.3	59.3	100
(iii)	100	100	-

MPC shows best results and is able to minimize the cost function more efficiently than standard MPC. The IAE is again significantly reduced in comparison to the PID, but this time the online-linearized MPC also clearly outperforms the standard MPC.

VI. CONCLUSION

We applied an adaptive MPC approach that is suited to control nonlinear hydraulic processes, without being more demanding on the computational hardware than standard online MPC. In contrast to existing online-linearization concepts, our approach re-linearizes the internal model only when the control setpoint is changed. It is straightforward to implement the proposed approach, since standard, linear MPC algorithms can be reused. We compared the performance of the propsed controller to a standard, linear MPC and to a PI/PID control on a by applying them to the simultaneous control of pressure and flow rate in a side-channel pump. Both MPC variants show a significantly increased control quality when compared to the PI/PID control. The proposed adaptive MPC outperforms the standard MPC whenever large deviations from the original operating point occur. In fact, linear MPC often fails in this case.

REFERENCES

P. Drews, K. Hoffmann, R. Beck, R. Gasper, A. Vanegas, C. Felsch, N. Peters and D. Abel. Fast model predictive control for the air path of a turbocharged diesel engine. *Proceedings of the European Control Conference (ECC), 2009*, pages 3377–3382. IEEE, 2009.

P. Falcone, F. Borelli, H. E. Tseng, J. Asgari and D. Hrovat. Linear timevarying model predictive control and its application to active steering systems: Stability analysis and experimental validation. *International journal of robust and nonlinear control*, 18.8 (2008): pages 862–875.

A. Gambier, A. Wellenreuther, and E. Badreddin. Optimal control of a reverse osmosis desalination plant using multi-objective optimization. *2006 IEEE Conference on Computer Aided Control System Design*, IEEE, 2006.

G. Grabow. Comparison of side-channel-, labyrinth- and jet-pumps (in German). *Forschung im Ingenieurwesen*, volume 62, pages 11–20. 1996.

J. F. Gulich. *Centrifugal pumps*, Springer, 2007.

L. C. Henriksen, and N. K. Poulsen. An online re-linearization scheme suited for Model Predictive and Linear Quadratic Control. *Technical University of Denmark, DTU Informatics, Building 321*, 2010.

J. M. Maciejowski. Predictive control: with constraints. *Pearson education*, 2002.

S. Skogestad and I. Postlethwaite. Multivariable feedback control: analysis and design. Vol. 2. New York: Wiley, 2007.

D. Surek. Design and projecting of side-channel- and peripheral-pumps (in German). *Forschung im Ingenieurwesen*, volume 63, pages 235–253. Springer, 1997.

Q. Wang and Y. Zhang. Robust identification of continous systems with dead-time from step responses. *Automatica*, volume 37, pages 377–390. Pergamon, 2001.